A time-of-flight powder neutron diffraction study of ternary chromium sulfides, $Ni_xCr_{3-x}S_4$ ($0 < x \leqslant 1.0$)

Douglas C. Colgan and Anthony V. Powell*

Department of Chemistry, Heriot-Watt University, Riccarton, Edinburgh, UK EH14 4AS

Time-of-flight powder neutron diffraction has been used to investigate the distribution of nickel and chromium cations between two crystallographically independent sites in the series of ternary sulfides, $Ni_xCr_{3-x}S_4$ ($0 < x \leqslant 1.0$). These materials are isostructural with Cr_3S_4 (space group $I2/m$: $a \approx 5.9$ Å, $b \approx 3.4$ Å, $c \approx 11.1$ Å, $\beta \approx 91.5°$) over the entire range of composition. At all values of x, nickel cations preferentially occupy sites in an ordered-vacancy layer with only a small percentage ($\leqslant 15\%$) residing at sites in a fully occupied metal layer. This distribution is close to that expected for the normal structure type. The absence of any significant dependence on x of the cation distribution is reflected in the magnetic properties, which show relatively little compositional variation. Electronic properties, however, indicate a change in the nature of the valence electrons with decreasing nickel content.

The Cr_3S_4 structure (Fig. 1), adopted by a large number of binary transition-metal chalcogenides of general formula M_3X_4, is one of a range of ordered-defect structures intermediate between the CdI_2 and NiAs structure types.[1] This structure may be considered to be derived from that of NiAs by removal, in an ordered manner, of half of the metal cations (M) from alternate metal layers, resulting in a change from the ..XMXMXMX.. stacking sequence found in NiAs, to one of ..XMXM$_{1/2}$XMX... This results in two crystallographically distinct cation sites, as indicated by the formulation (M)[M_2]X_4, where (M) and [M] denote sites in the vacancy and the fully occupied layers respectively. In a ternary chalcogenide, of formula M′M_2X_4, two extreme cation arrangements are possible.[2] These correspond to the normal (M′)[M_2]X_4 and inverse (M)[M′M]X_4 structures.

In addition to stoichiometric ternary phases, a number of non-stoichiometric phases $M'_xM_{3-x}S_4$ have been synthesised[3–11] and found to exhibit variations in physical properties as a function of composition. Our interests have focused on efforts to modify systematically, the electronic and magnetic properties of materials of the Cr_3S_4 structure type by suitable chemical substitution. We have recently reported a study of the structural and physical properties of the non-stoichiometric series $V_xCr_{3-x}S_4$ ($0 \leqslant x \leqslant 1.0$)[3,4] for which the end members show contrasting magnetic and electronic properties. Whereas Cr_3S_4 is metallic, and orders antiferromagnetically with a Néel temperature of $T_N \approx 200$ K,[12] our own measurements indicate semiconducting VCr_2S_4 to be a magnetically frustrated system, best regarded as a spin-glass. Compositionally induced changes in physical properties were observed in this series and it has been shown[4,13] that these changes are accompanied by a change in the relative site preferences of the two cations.

In seeking to extend this study, we have recently prepared ternary phases $Ni_xCr_{3-x}S_4$ ($0 \leqslant x \leqslant 1.0$), containing Ni^{II}, the d^{n+5} analogue of V^{II}. On the basis of one-electron one-molecule energy level diagrams (Fig. 2), of the type presented by Holt *et al.*,[14] semiconducting behaviour is predicted for the end-member phase $NiCr_2S_4$. Examination of this diagram suggests that the electron count associated with the (M)-site cation can be continuously varied by progressive substitution of Ni^{II} with Cr^{II}. In particular, preparation of $Ni_xCr_{3-x}S_4$ phases in intervals of $x = 0.25$ over the range $0 \leqslant x \leqslant 1.0$ provides a means of changing the formal electron count by one for each step in composition. Using this strategy, we sought to investigate changes in structural and physical properties between metallic Cr_3S_4 and semiconducting $NiCr_2S_4$. The results of these investigations are presented below.

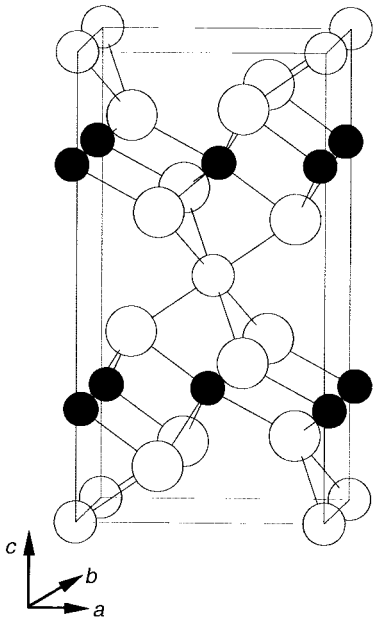

Fig. 1 A ball and stick representation of the Cr_3S_4 structure. Small filled circles represent cations in the fully occupied layer, small open circles represent cations in the vacancy layer and large open circles represent anions.

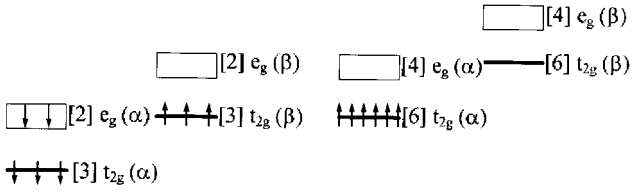

Fig. 2 Schematic one-electron one-molecule energy level diagram for $NiCr_2S_4$. Levels to the left correspond to the divalent ion, those to the right to the trivalent ion. Numbers in brackets signify the total degeneracy of a level. Intra-atomic exchange removes the degeneracy of the two spin states labelled α and β. Occupancies are given for the normal structure type.

Experimental

All samples of $Ni_xCr_{3-x}S_4$ ($0 \leqslant x \leqslant 1.0$), in increments of $x = 0.25$, were prepared by standard high-temperature ceramic synthesis. Appropriate quantities of high-purity nickel (99.99%), chromium (99.5%) and sulfur (99.999%) powders (all Aldrich) were ground in an agate mortar and pestle prior to loading into silica ampoules and sealing under vacuum (*ca.* 10^{-4} mbar). All reaction mixtures were prepared with a slight deficiency of sulfur corresponding to compositions $(Ni,Cr)_3S_{3.94}$, as it has been shown[1] that the phase range of Cr_3S_4 does not extend to the fully stoichiometric composition. Mixtures were fired at 1173 K for 24 h, before being reground and refired twice at 1273 K for 3 days with intermittent regrinding. In all cases, ampoules were cooled to 773 K before removal from the furnace. Reaction progress was monitored by powder X-ray diffraction using a Philips PA2000 diffractometer with nickel-filtered Cu-Kα radiation. Rietveld refinement was used for initial structural characterisation using data collected in step-scan mode at 2θ increments of 0.02° and a counting time of 5 s per step.

Energy dispersive X-ray microanalysis, to determine Ni : Cr ratios, was carried out using a JEOL 200FX electron microscope fitted with a Tracor Northern analysis system. $NiCr_2O_4$, prepared *via* the precursor route of Whipple and Wold,[15] was used as an intensity standard. Thermogravimetric analysis, performed under a flow of dry air, on a Stanton Redcroft STA-780 series thermoanalyser was used to determine sulfur contents. The weight loss on conversion to the appropriate oxides is related directly to the sulfur content.

Magnetic susceptibility data were collected for powdered samples using a Quantum Design MPMS2 SQUID susceptometer. Samples were loaded into gelatin capsules at room temperature and data were collected over the temperature range $3 \leqslant T/K \leqslant 296$ both after cooling the sample in zero applied field (zfc) and after cooling in the measuring field (fc) of 1 kG. Data were corrected for the diamagnetism of the gelatin capsule and for intrinsic core diamagnetism. The electrical resistance of the sample was measured using the four-probe dc technique. An ingot (*ca.* $6 \times 3 \times 1$ mm) was cut from a sintered pellet, four 50 μm silver wires were attached using colloidal silver paint and connections were made to an HP34401A multimeter. Measurements over the temperature range $80 \leqslant T/K \leqslant 400$ were made by placing the sample in an Oxford Instruments CF1200 cryostat connected to an ITC502 temperature controller.

Room-temperature time-of-flight powder neutron diffraction data were collected on the LAD neutron diffractometer, at the ISIS spallation neutron source, Rutherford Appleton Laboratory, Oxon. Samples (*ca.* 2 g) were loaded into thin-walled vanadium cans. Preliminary data reduction was carried out on the Rutherford Appleton Laboratory VAX 4500/4300 computer using Genie[16] spectrum manipulation software. Rietveld refinement was performed using the GSAS[17] suite of programs installed on the Heriot-Watt University DEC Alpha 2100–4725 system.

Results

Chemical analysis (Table 1) indicates that sample compositions are in good agreement with the stoichiometry of the initial reaction mixtures. Initial structural characterisation, by powder X-ray diffraction, reveals that all materials are single phases isostructural with Cr_3S_4. Rietveld refinement of X-ray diffraction data yielded unit-cell parameters similar to those previously reported for related phases.[18] A contraction in unit-cell volume is observed as the extent of nickel substitution is increased. Cell parameters for the ternary phase $NiCr_2S_4$ are all smaller than those reported by Jellinek.[1]

Magnetic susceptibility data (Fig. 3) throughout the composition range show a weak temperature dependence, similar to that previously reported[19,20] for $NiCr_2S_4$. At low nickel contents ($x \leqslant 0.5$), zfc and fc curves overlie each other completely, at all but the lowest temperatures studied. Zfc and fc data for $Ni_{0.75}Cr_{2.25}S_4$ show a slight divergence over the entire temperature range, whereas those for $NiCr_2S_4$ diverge only below *ca.* 60 K. Electrical data (Fig. 4) demonstrate that although all materials possess similar room-temperature resistivities, the temperature dependence of that of the end-member phase differs from that of the other materials. In particular, whereas all non-stoichiometric materials exhibit a decrease in resistivity on cooling below *ca.* 325 K, that of $NiCr_2S_4$ shows a more complex temperature dependence.

Neutron data, from the highest resolution backscattering bank of detectors ($2\theta = 145°$), in the time-of-flight range 2000–18 000 μs ($d = 0.40$–3.35 Å) were summed and normalised. Neutron scattering lengths incorporated in the GSAS package were utilised. The initial structural model, using atomic coordinates determined in our previous study of Cr_3S_4, involved nickel occupying sites exclusively in the vacancy layer [2(a); 0,0,0]. A shifted Chebyshev polynomial, with the coefficients included as refinable parameters, was used to model the neutron background and a Gaussian convoluted with two back-to-back exponentials was used to describe the peak shape.

After initial refinement of a scale factor, background and lattice parameters, two weak features which were not fitted by our structural model were apparent in the range $d = 2.1$–2.2 Å. These features had previously been identified[4] as the (110) reflection of vanadium ($d_{calc} = 2.141$ Å), instrumental in origin, and the (113) reflection of Cr_2O_3 ($d_{calc} = 2.173$ Å), possibly present as a result of attack of the silica ampoule. When Cr_2O_3 was included as a second phase, an estimate of $<2\%$ by weight of the oxide impurity was obtained. This is below the limit of detection by our powder X-ray diffractometer, which accounts for the absence of reflections arising from Cr_2O_3 in the X-ray diffraction patterns. There was no significant improvement in the quality of the refinement and no change in the refined parameters when the second phase was included. Consequently, data in the region 11 300–12 000 μs ($d = 2.10$–2.24 Å) were excluded from all refinements. Subsequent refinement of atomic coordinates and thermal parameters proceeded smoothly. Finally, site-occupancy factors were

Table 1 Results of thermogravimetric analysis and energy dispersive X-ray microanalysis for $Ni_xCr_{3-x}S_4$ phases

nominal composition	nominal Ni:Cr	experimentally determined Ni:Cr	experimentally determined S:(Ni + Cr)	experimentally determined composition[a]
$Ni_{0.25}Cr_{2.75}S_{3.93}$	0.09	0.09(1)	1.31(1)	$Ni_{0.25}Cr_{2.75}S_{3.93}$
$Ni_{0.5}Cr_{2.5}S_{3.93}$	0.20	0.20(2)	1.32(1)	$Ni_{0.5}Cr_{2.5}S_{3.96}$
$Ni_{0.75}Cr_{2.25}S_{3.93}$	0.33	0.35(2)	1.31(1)	$Ni_{0.78}Cr_{2.22}S_{3.92}$
$NiCr_2S_{3.93}$	0.50	0.51(3)	1.30(1)	$Ni_{1.01}Cr_{1.99}S_{3.91}$

[a]Normalised to a total metal content of three.

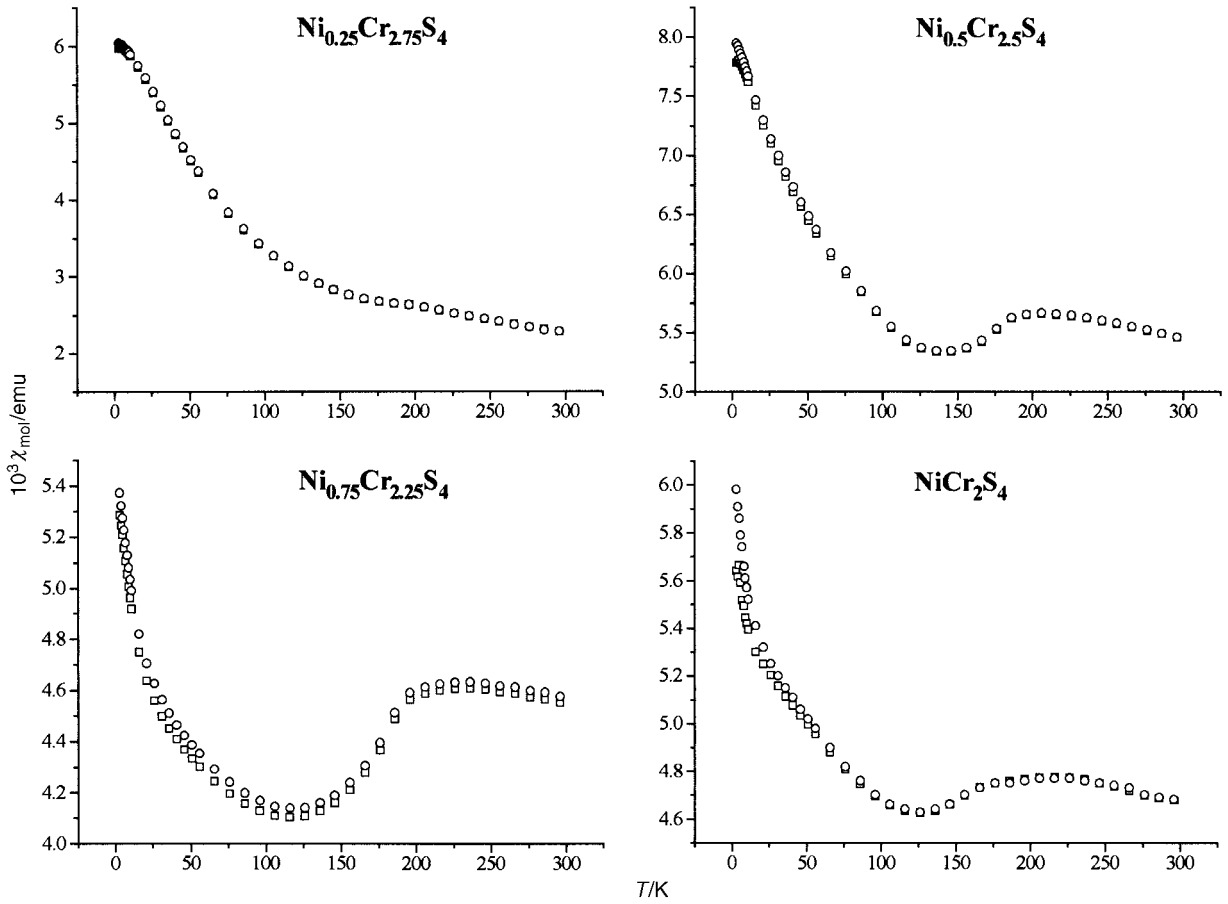

Fig. 3 Zero-field-cooled (zfc, □) and field-cooled (fc, ○) molar magnetic susceptibilities for $Ni_xCr_{3-x}S_4$ phases measured in a field of 1 kG

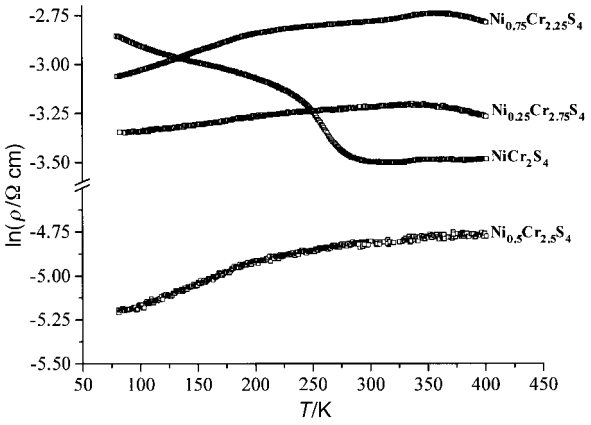

Fig. 4 Temperature dependence of the electrical resistivity of $Ni_xCr_{3-x}S_4$ phases

introduced into the refinement, with the constraint that overall stoichiometry be maintained. This led to an improvement in the quality of the fit. However, some intensity mismatches remained at long times-of-flight. These were found to be correlated to nickel content and were initially attributed to an absorption problem. However, neither introduction and refinement of an absorption coefficient nor correction of the raw data for absorption led to an improvement in the fit. The origin of this problem is still not currently understood, but may be instrumental, arising from poor modelling of the peak shape at long times-of-flight.

Final observed, calculated and difference profiles are shown in Fig. 5 and refined parameters are given in Table 2. Selected bond lengths and angles may be found in Tables 3 and 4.

Discussion

The magnetic and electronic properties of $NiCr_2S_4$ have been discussed previously,[21] in conjunction with the results of a variable-temperature powder neutron diffraction study, which demonstrated that the decrease in susceptibility at *ca.* 200 K is associated with the onset of long-range magnetic order. The increase in magnetic susceptibility at lower temperatures may be traced to different temperature dependences of cation moments on the two sub-lattices. Failure to fit susceptibility data in the high-temperature region to a Curie–Weiss law, even with incorporation of a temperature-independent term, suggests that a localised-electron model is not wholly applicable to this system; a view which is supported by the observation of a low, temperature-independent resistivity above 300 K. Although some caution is required in interpreting resistivity data obtained on sintered pellets owing to contributions from grain boundaries, data below 300 K indicate that $NiCr_2S_4$ is a low activation energy semiconductor whose activation energy decreases below the magnetic ordering temperature. By contrast, electronic properties of the non-stoichiometric materials suggest the presence of delocalised electrons. However, for the $x=0.25$ and $x=0.75$ phases, $d(\ln\rho)/dT$ appears to change sign at higher temperatures (>375 K). This suggests that these materials are in close proximity to a boundary between localised and delocalised behaviour. These temperatures are unfortunately at the limits of operation of our current equipment and this factor has, to

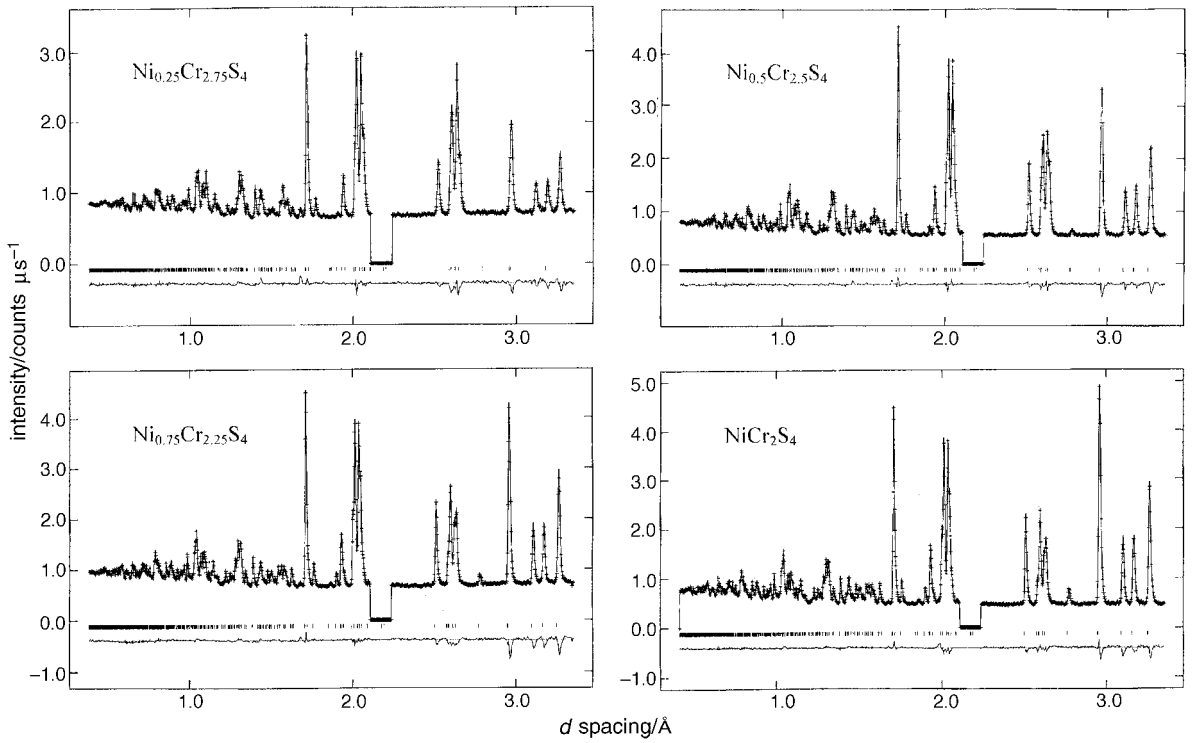

Fig. 5 Final observed (crosses), calculated (full line) and difference (lower full line) neutron profiles for $Ni_xCr_{3-x}S_4$ phases. Reflection positions are marked.

Table 2 Refined parameters for $Ni_xCr_{3-x}S_4$ phases[a]

		x in $Ni_xCr_{3-x}S_4$			
		0.25	0.50	0.75	1.0
	a/Å	5.9392(3)	5.9222(2)	5.9103(1)	5.9082(2)
	b/Å	3.4173(2)	3.4145(1)	3.4133(1)	3.4138(1)
	c/Å	11.1740(5)	11.1193(3)	11.1022(3)	11.0815(3)
	β/°	91.464(2)	91.337(2)	91.341(2)	91.363(2)
(M)	SOF[b] Ni	0.241(5)	0.476(4)	0.713(5)	0.852(4)
	SOF Cr	0.759(5)	0.524(4)	0.287(5)	0.148(4)
	B/Å^2	0.58(4)	0.58(3)	0.55(3)	0.44(2)
[M]	SOF Ni	0.004(2)	0.012(2)	0.019(2)	0.074(2)
	SOF Cr	0.996(2)	0.988(2)	0.981(2)	0.926(2)
	x	−0.0236(3)	−0.0230(2)	−0.0220(3)	−0.0204(2)
	z	0.2597(2)	0.2602(1)	0.2611(1)	0.2602(2)
	B/Å^2	0.44(4)	0.46(3)	0.36(3)	0.37(3)
S(1)	x	0.3414(4)	0.3419(3)	0.3425(4)	0.3423(3)
	z	0.3659(2)	0.3659(2)	0.3658(2)	0.3660(2)
	B/Å^2	0.17(2)	0.23(1)	0.11(1)	0.16(1)
S(2)	x	0.3331(4)	0.3314(3)	0.3307(4)	0.3294(3)
	z	0.8804(2)	0.8810(2)	0.8808(2)	0.8804(2)
	B/Å^2	0.17(2)	0.23(1)	0.11(1)	0.16(1)
R_{wp} (%)		1.7	1.7	2.0	1.9
χ^2		3.3	3.9	4.4	3.4

[a]Space group: $I2/m$, (M) on 2(a) (0,0,0), [M] on 4(i) (x,0,z), S(1) and S(2) on 4(i) (x,0,z). [b]SOF: site-occupancy factor.

date, prevented further study of the high-temperature electronic properties of these materials.

Magnetic data for the non-stoichiometric phases are qualitatively similar to those for $NiCr_2S_4$, although the long-range order in $Ni_{0.25}Cr_{2.75}S_4$ manifests itself in a discontinuity in $\chi(T)$ rather than a decrease in susceptibility. Powder neutron diffraction data confirm that all materials adopt a low-temperature magnetically ordered structure similar to that proposed for $NiCr_2S_4$ by Andron and Bertaut.[22] However, differences in behaviour at intermediate temperatures are observed. In particular, the non-stoichiometric materials exhibit more complex behaviour involving spin-reorientation around 100 K. The magnetic neutron scattering experiments will be described in full elsewhere.[23]

The smooth decrease in the a and c lattice parameters as the extent of nickel substitution is increased (Fig. 6) is in accord with the smaller ionic radius of nickel [$r(Ni^{2+})=0.69$ Å, $r(Cr^{2+})=0.80$ Å].[24] Metal cations at both crystallographic sites lie at the centres of distorted octahedra, with sites in the fully occupied layer being more distorted than those in the

Table 3 Selected bond distances (Å) for $Ni_xCr_{3-x}S_4$ phases

	x in $Ni_xCr_{3-x}S_4$			
bond	0.25	0.50	0.75	1.0
M(1)—S(1)	2.445(2) × 4	2.439(1) × 4	2.436(2) × 4	2.434(1) × 4
M(1)—S(2)	2.416(2) × 2	2.393(2) × 2	2.386(2) × 2	2.380(2) × 2
mean M(1)—S	2.44	2.42	2.42	2.42
M(2)—S(1)	2.445(3)	2.436(2)	2.424(3)	2.408(2)
	2.477(2) × 2	2.470(2) × 2	2.496(2) × 2	2.471(2) × 2
M(2)—S(2)	2.384(3)	2.380(2)	2.383(3)	2.385(2)
	2.350(2) × 2	2.349(2) × 2	2.343(2) × 2	2.341(2) × 2
mean M(2)—S	2.41	2.41	2.41	2.40
M(1)—M(2)	2.909(2) × 2	2.899(1) × 2	2.905(2) × 2	2.909(1) × 2
M(2)—M(2)	3.189(3) × 2	3.189(2) × 2	3.194(3) × 2	3.211(2) × 2
	3.683(3) × 2	3.668(3) × 2	3.654(3) × 2	3.638(2) × 2

Table 4 Selected bond angles (°) for $Ni_xCr_{3-x}S_4$ phases

	x in $Ni_xCr_{3-x}S_4$			
angle	0.25	0.50	0.75	1.0
S(1)—M(1)—S(1)	88.66(8) × 2	88.85(6) × 2	88.95(8) × 2	89.08(7) × 2
	91.34(8) × 2	91.15(6) × 2	91.05(8) × 2	90.92(7) × 2
S(1)—M(1)—S(2)	88.23(7) × 4	88.28(5) × 4	88.12(6) × 4	88.08(5) × 4
	91.79(7) × 4	91.72(5) × 4	91.88(6) × 4	91.92(5) × 4
S(1)—M(2)—S(1)	83.13(9) × 2	83.22(7) × 2	83.37(8) × 2	83.59(7) × 2
	87.22(1)	87.46(7)	87.48(9)	87.40(7)
S(1)—M(2)—S(2)	92.91(9) × 2	93.28(7) × 2	93.76(9) × 2	94.40(7) × 2
	89.63(5) × 2	89.55(5) × 2	89.46(6) × 2	89.45(5) × 2
	88.21(9) × 2	87.85(7) × 2	87.44(8) × 2	87.12(6) × 2
S(2)—M(2)—S(2)	95.31(9) × 2	95.21(6) × 2	94.96(8) × 2	94.39(6) × 2
	93.29(1)	93.26(9)	93.48(11)	93.65(9)

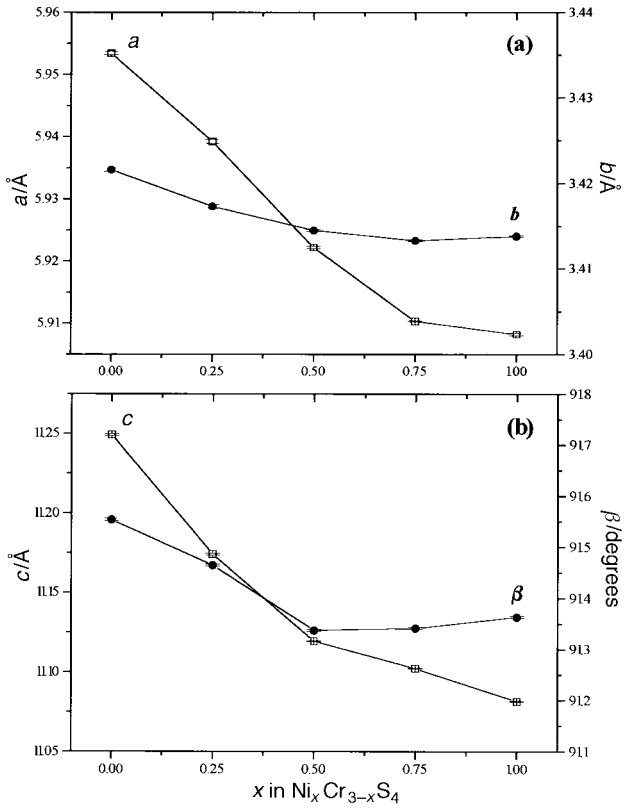

Fig. 6 The compositional dependence of the unit cell parameters of $Ni_xCr_{3-x}S_4$: (a) a and b parameters, (b) c and β parameters. Data for Cr_3S_4 are taken from ref. 4.

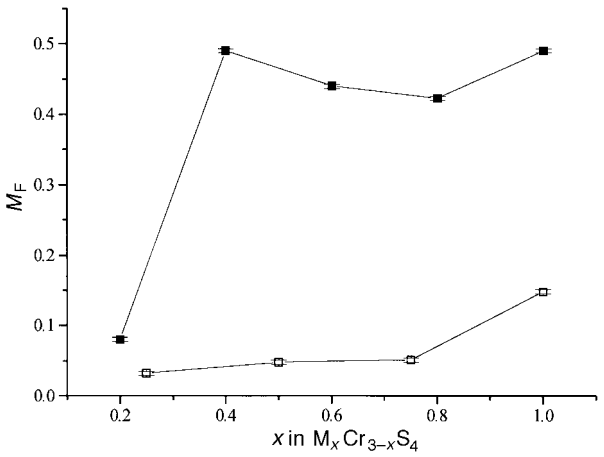

Fig. 7 The compositional dependence of the fraction, M_F, of M in $M_xCr_{3-x}S_4$ residing in the fully occupied layer. Solid points for M = V, open points for M = Ni.

vacancy layer. Cations in the vacancy layer, M(1), have four long and two short bonds to sulfur. Although the average M(1)—S bond length shows little variation with the extent of nickel substitution, the extent of the distortion increases, as reflected in the increase in the ratio of the long to short bond length. Similarly cation sites, M(2), in the fully occupied layer show little variation in M(2)—S bond lengths as nickel incorporation is varied. However, a larger variation in S—M(2)—S bond angles is observed than for S—M(1)—S, which are all close to 90°. Mean cation–anion separations of *ca.* 2.4 Å are consistent with the sum of respective ionic radii.[24]

All materials investigated adopt structures which closely approach the normal type $\{(M')[M_2]X_4\}$. However, at all compositions, a small fraction of nickel cations reside in sites in the fully occupied layer. This fraction is relatively insensitive to nickel content, although that in the stoichiometric end-member phase $NiCr_2S_4$ is slightly greater than expected by extrapolation from the non-stoichiometric members of the series. The cation distribution in $NiCr_2S_4$, determined in this study, is in excellent agreement with that recently established from more limited angle-dispersive powder neutron diffraction data during the course of an investigation of magnetic ordering in $NiCr_2S_4$.[21]

The adoption of what is essentially a normal structure type is in agreement with previous assumptions concerning the structure of stoichiometric MCr_2S_4 (M = Ti, V, Cr, Ni)[2] ordered-defect phases. However, the relatively few detailed structural investigations which have been performed demonstrate that such assumptions are not always valid. For example, a combination of powder X-ray and neutron diffraction data[13] has shown that in VCr_2S_4 vanadium cations are distributed between the two octahedral sites, corresponding to the formulation $(V_{0.51}Cr_{0.49})[V_{0.49}Cr_{1.51}]S_4$, contrary to the previously assumed structure.[2] Powder neutron diffraction has established[25] that a similar distribution pertains in the analogous selenide VCr_2Se_4. In the same study, it was shown that in VTi_2Se_4, vanadium exhibits a slight preference for sites in the vacancy layer. A more marked site preference is observed[26] in $TiCr_2Se_4$ and $CrTi_2Se_4$, where chromium preferentially occupies sites in the vacancy layer. FeV_2S_4 and VFe_2S_4 appear to be the only examples, containing later transition-series cations, for which cation distributions have been investigated. In both cases, powder neutron diffraction data reveal[27] that there is a marked preference for vanadium to occupy sites in the fully occupied layer. In VFe_2S_4, this preference is sufficiently marked to lead to almost complete partitioning and the adoption of a near-inverse structure type $\{(Fe_{0.94}V_{0.06})[Fe_{1.04}V_{0.96}]S_4\}$.

On the basis of these studies, it may be concluded that the preference for sites in the fully occupied layer decreases in the order $Ti > V \approx Cr > Fe$. The structure of $NiCr_2S_4$ appears to continue this trend with approximately 15% of the nickel cations found on sites in the fully occupied layer, which compares to 26% of iron cations in FeV_2S_4. This change in site preference reflects the relative abilities of transition-series cations to delocalise electrons by direct t_{2g}–t_{2g} overlap. Goodenough has suggested[28] that there is a critical separation, R_c, below which direct orbital overlap is possible. On traversing the transition series, overlap between cation orbitals becomes less effective for a given cation–cation separation owing to the effects of orbital contraction. Consequently, there is a decrease in R_c on traversing the series, and cations drawn from the earlier part of the series exhibit stronger t_{2g}–t_{2g} interactions. The two octahedral sites in the Cr_3S_4 structure differ in the number of intra-layer nearest neighbour cations. The six neighbours in the fully occupied layer provide greater opportunity for electron delocalisation than the two intra-layer neighbours in the vacancy layer. We have suggested[4] that it is this which is responsible for the preferential occupation of sites in the fully occupied layer by early transition-series cations. When the two cations present are drawn from groups which are well separated in the transition series, this preference is sufficiently marked to lead to almost complete partitioning, as is observed in VFe_2S_4 and $NiCr_2S_4$. However, cations which are adjacent in the transition series have similar values of R_c. This leads to less marked site preferences in materials containing cations from neighbouring groups, and results in structures intermediate between the normal and inverse types. In such structures, the cation distribution is that which best balances the competition between electron delocalisation and the charge separation introduced by the incorporation of a divalent ion into the fully occupied layer.

The cation distribution in the non-stoichiometric materials is composition dependent. It is instructive to compare this dependence for the $Ni_xCr_{3-x}S_4$ series determined here with that of the $V_xCr_{3-x}S_4$ series,[4] for which very different behaviour is observed (Fig. 7). In the latter series, vanadium is almost equally apportioned between the two octahedral sites in the composition range $0.4 \leqslant x \leqslant 1$. The fraction of vanadium in the fully occupied layer is close to the ideal value of 0.5 expected for such a distribution. A marked change occurs below $x = 0.4$, and in $V_{0.2}Cr_{2.8}S_4$ almost all of the vanadium present resides at sites in the vacancy layer. This change in the distribution occurs in the same composition range as that in which changes in physical properties and anomalies in the composition dependence of cell parameters are observed.[3] By contrast, the distribution in the nickel series is less sensitive to composition and only a small amount of nickel is present in the fully occupied layer throughout the composition range. This influences the composition dependence of physical properties which show more gradual changes than those for the analogous vanadium-containing series. In particular, magnetic ordering and itinerant electron behaviour are observed over a much wider range of composition.

Financial support from the EPSRC (grants GR/J36075 and GR/J34231) and The Royal Society is gratefully acknowledged. The authors wish to thank Dr. K. S. Knight, Rutherford Appleton Laboratory, and Dr. A. M. Chippindale, University of Oxford, for assistance with the collection of neutron diffraction data and energy dispersive microanalysis data respectively. D. C. C. thanks Heriot-Watt University for a studentship.

References

1 F. Jellinek, *Acta Crystallogr.*, 1957, **10**, 620.
2 A. Wold and K. Dwight, *Solid State Chemistry: Synthesis, Structure and Properties of Selected Oxides and Sulfides*, Chapman and Hall, New York, 1993, ch. 11.
3 A. V. Powell and S. Oestreich, *J. Mater. Chem.*, 1996, **6**, 807.
4 D. C. Colgan and A. V. Powell, *J. Mater. Chem.*, 1996, **6**, 1579.
5 Y. Tazuke, *J. Phys. Soc. Jpn.*, 1981, **50**, 413.
6 Y. Tazuke, K. Wantanabe and T. Suzuki, *J. Phys. Soc. Jpn.*, 1981, **50**, 2900.
7 S. Ohta, A. Fujii and S. Anzai, *J. Phys. Soc. Jpn.*, 1983, **52**, 1765.
8 S. Ohta, *J. Phys. Soc. Jpn.*, 1983, **54**, 1076.
9 Y. Sugimoto, S. Ohta, S. Yuri, M. Tamaki and S. Anzai, *J. Phys. Soc. Jpn.*, 1985, **54**, 3240.
10 Y. Ueda, K. Kosuge, M. Urabayashi, A. Hayashi, S. Kachi and S. Kawano, *J. Solid State Chem.*, 1985, **56**, 263.
11 H. Nozaki and H. Wada, *J. Solid State Chem.*, 1983, **47**, 69.
12 D. Babot, M. Chevreton, J. L. Buevoz, R. Langier, B. Lambert-Andron and M. Wintenberger, *Solid State Commun.*, 1979, **30**, 253.
13 A. V. Powell and D. C. Colgan, *Mater. Sci. Forum*, 1996, **228**, 831.
14 S. L. Holt, R. J. Bouchard and A. Wold, *J. Phys. Chem. Solids*, 1966, **27**, 755.
15 E. Whipple and A. Wold, *J. Inorg. Nucl. Chem.*, 1962, **24**, 23.
16 W. I. F. David, M. W. Johnson, K. J. Knowles, C. M. Moreton-Smith, G. D. Crosbie, E. P. Campbell, S. P. Graham and J. S. Lyall, *Rutherford Appleton Laboratory Report*, 1986, RAL-86-102.
17 A. C. Larson and R. B. von Dreele, *General Structure Analysis System, Los Alamos National Laboratory Report*, 1994, LAUR 86–748.
18 R. J. Bouchard and A. Wold, *J. Phys. Chem. Solids*, 1966, **27**, 591.
19 R. E. Tressler and V. S. Stubican, *J. Am. Ceram. Soc.*, 1968, **51**, 391.
20 B. L. Morris, P. Russo and A. Wold, *J. Phys. Chem. Solids*, 1970, **31**, 635.
21 A. V. Powell, D. C. Colgan and C. Ritter, *J. Solid State Chem.*, in press.
22 B. Andron and E. F. Bertaut, *J. Phys.* (*Paris*), 1966, **27**, 619.
23 A. V. Powell, D. C. Colgan and C. Ritter, manuscript in preparation.
24 R. D. Shannon, *Acta Crystallogr.*, *Sect. A*, 1976, **32**, 751.

25 A. Hayashi, K. Ueda, K. Kosuge, H. Murata, H. Asano, N. Watanabe and F. Izumi, *J. Solid State Chem.*, 1987, **71**, 237.
26 A. Hayashi, K. Ueda, K. Kosuge, H. Murata, H. Asano, N. Watanabe and F. Izumi, *J. Solid State Chem.*, 1987, **67**, 346.
27 J. M. Newsam, Y. Endoh and I. Kawada, *J. Phys. Chem. Solids*, 1987, **48**, 607.
28 J. B. Goodenough, *Magnetism and the Chemical Bond*, Wiley, New York, 1963.

Paper 7/02814H; *Received* 24*th April*, 1997